3D FEM STUDY ON AN AUSTENITIC STAINLESS STEEL FOR VERIFICATION THE ENGINEERING TREATMENT MODEL (ETM)

A. Cornec, G. Lin, K.-H. Schwalbe *)

3D constraint effects of finite thick specimens on the CTOD-δ_5 driving force are studied by FEM on stationary cracks. The deviation margins between 3D and 2D conditions will be presented. For most cases, i.e. where the ligament is 2 times larger or more than the thickness, the difference between inside and outside is weakly exhibited that δ_5 can be approximated to be constant versus thè thickness. A promising idea of simplification the analytical δ_5 driving force determination for 3D with the ETM construction will be presented. An example of the ETM demonstrates that the characteristics of the δ_5 driving force curves can be properly described by the current ETM construction based on 2D plane stress condition.

INTRODUCTION

The Engineering Treatment Model (ETM) is part of an assessment flaw procedure in order to estimate or predict analytically the load-deformation behaviour of cracked components. A first version of ETM (ETM/1-91) is given in (1). The current extented version (ETM/2-93) is still under preparation but has been verified on some examples (2)-(4). The ETM consits on different independ parts of analytical or numerical solutions, which will be condensed together to a whole construction. The constraint influence in finite thicknesses during the elastic-plastic loading interacts with several geometry and hardening parameters and cannot be considered accurately at time. The main interest with the ETM is directed to the crack opening displacement δ_5 which can be measured directly and can be used as a promising fracture parameter (5). Since the 3D effects are not yet systematically understood, more information is nessessary to improve the current existing estimation procedures. In this study the 3D constraint effects at stationary cracks has been investigated numerically by FEM on typical standard geometries (CT and CCT) with two distinct limiting thicknesses: relative thin (B = 5 mm) and relative thick (B = 25 mm). With this parameters the 3Dconstraint influence especially on δ_5 can be enclosed and some quantitive results can be drawn for the margins of deviations from the ETM estimation based on 2D plane stress conditions.

*) GKSS Research Centre Geesthacht, Max Planck Straße, D-21502 Geesthacht

ETM TREATMENT OF THE MATERIAL CURVE

An austenitic steel (X6CrNi1811 or AISI 316 respectively) has been considered in the study.and is a typical material class with a wide spread area of applications. Fig. 1 shows the true stress-strain curve. For the ETM application (version ETM/2-93) a specific treatment is nessessary to fit the arbitrary material curve by power laws.

The procedure is given briefly as follows: The first and the second hardening part of the material curve was determined by a regression program, where n_1 is fixed through point P and n_2 through point G*. The experience shows that in most cases the first hardening part has an effective hardening exponent, n_4, which is smaller than n_1. The average $n_4 = (n_1 + n_2)/2$ is an good approximation, where n_3 is like an upper bound for the first hardening part of the δ_5 driving force and can be determined easily by the fix-points P and G*. The intersection point of the power law with the inital elastic compliance gives the reference yield stress σ_0 which is nessessary to fix the power laws in the ETM construction. The following values has been determined, which all are at last fixed by the two points P and G*.

E-Modul (MPa)	$R_{p0.2}$ (MPa)	R_m (MPa)	R_m^* (MPa)	$\varepsilon_{0.2}^*$	ε_m^*	ε_m^*
195000	238.8	617	988	0.003224	0.60126	0.4708

n_1	n_2	n_3	n_4	σ_{01} (MPa)	σ_{03} (MPa)	σ_{04} (MPa)
6.0901	2.0942	3.5096	4.8000	197.436	15.7088	185.089

3D SITUATION

The 3D FEM results are restricted here only on the δ_5 driving force, which is measured at 2.5 mm distance rectangular and versus the crack front quite analog to the experimental technique. Additionaly the 2D limiting cases plane strain (upper bound on the load scale) and plane stress (lower bound) are also considered.

For CT specimens Fig. 2a shows δ_5 at $z' = z/(B/2) = 0$ (inside) compared to $z' = 1$ (outside) during the loading up to the fully plastic regime. The difference of this relation increases with thickness. Besides the absolute thickness, B, it seems better to introduce the ligament slenderness, B/L, as a controlling constraint parameter. The value B/L = 1 means a square area, which exhibits a higher constraint influence on δ_5 than small B/L values. In Fig. 2a for B = 25 mm (or B/L = 1) significant difference occurs between inside and outside, which increases during the increasing load, much more than for thin specimens. With this, the following statement should be noted, that for equal B/L values the same constraint situation should be expected, which is contrary to an absolute thicknes correlation. This statement will be proved otherwise for B/L = 1 with different thicknesses.

Using an average value for δ_5 versus the thickness, Fig. 2b, the constraint dependence is than highly reduced below a 10% margin. That means with other words, the δ_5 versus the thickness is for the most part near by the inside situation. The δ_5 dependence for B = 25 mm has a parabolic type from inside to outside. Much smaller thickness dependence can be observe on the CCT specimens, Fig. 3, where no significant differences occur between inside and outside for the whole B/L range ($0 \leq B/L \leq 1$).

Thus for austenitic steels the thickness 3D constraint situation with respective to δ_5 is only weakly effected by different thicknesses. For CT specimens with square ligaments (B/L = 1) the crack iniation, starting at inside, but measured experimentally by $\delta_{5outside}$ can occur below compared to respective CCT specimens. From the existing experimental results, however, such behaviour has not yet observed as significant beyond the typical scatter band. Probably, as the experimentally fatigued crack front is normaly continousely curved, typically in a thumnail form, where the difference inside/outside can be smaller than for a straight crack front.

The characteristics of the δ_5 driving force can be seen at the best in a normalized ETM diagramm (log-log scale). Fig. 4 for CCT and Fig. 5 for CT show the normalized δ_5 curves together with the 2D limiting cases. It is interested to see, that all δ_5 curves are congruent and differ over the whole loading range by a constant logarithmic shift. This leads to the idea, to determine the individual 3D δ_5 values only at the limit load (or near by), because the following part of the plastic curve is the same as for the plane stress reference case. For the large strain theory (LST) especially for the 2D plane stress case, a significant deviation in the δ_5 driving force curves compared to the small strain theory (SST) can be observed in the second hardening part at high load levels, Fig. 4, 5. For 3D cases this effect takes place much later, so that the SST can be used further in the interested region of application. This is an important statement, because the ETM is based on the SST.

Fig. 6 shows the ETM construction (version ETM/2-93) for CT specimens as an verification example. The ETM details are to extensive to describe them all. Information can be found in (2)-(5). A good coincidence with the 3D cases as a lower bound estimation can be stated. This is mainly due to the use of fully plastic solutions in ETM/2-93, which guarantee a good approximation in the plastic loading regime.

CONCLUSIONS

The following conclusions and statements of 3D constraint effects espially on the δ_5 driving force specified for austenitic materials can be drawn:

- For CCT specimens the 3D effects between inside/outside can be neglected.
- For CT specimens the 3D effects between inside/outside appear only about $B/L \approx 1$ (square ligaments). For values $B/L \leq 0.5$ the 3D effects can be ingnored.

- The 3D δ_5 driving force curves are all congruent together and can be shifted in the 2D plane stress solution only by the indididual 3D δ_5 value at the net section yield load. This can be a key for a better considering 3D situations on δ_5.
- With the new ETM as a general valid construction δ_5 can due to the small 3D effects be properly described by the 2D plane stress case with high accuray.

SYMBOLS USED

CTOD	=	crack tip opening displacement
CT	=	Compact Tension specimen, standard fracture test specimen
CCT	=	Centred Cracked Tension Panel
a_{eff}	=	effective crack length including the plastic zone size
n	=	hardening exponent
B	=	thickness
B/L	=	ligament slenderness
L	=	ligament length
F	=	load
$F_{Y0.2\text{-}2D}$	=	yield load at net section
δ_5	=	crack driving force; ±2.5 mm rectangular from the crack tip
$\delta_{5Y0.2\text{-}2D}$	=	δ_5 corresponding to $F_{Y0.2\text{-}2D}$
$\delta_{5inside}$	=	δ_5 at inside, $z = 0$
$\delta_{5outside}$	=	δ_5 at outside (surface), $z = B/2$
δ_{SSY}	=	analytical formular for estimation δ_5 at the net secion yield load
σ_0	=	reference yield stress

REFERENCES

(1) Schwalbe, K.-H.and Cornec, A., Fat. Fract. Engng. Mater. Structures, Vol. 14, 1991, pp. 405-412.

(2) Cornec, A., Bauschke, H.-M., Anwendung des Engineering Treatment Model (ETM) bei zugbeanspruchten Strukturen mit Oberflächenrissen. Technical Note GKSS/WW/91/12, 1991, GKSS Research Center Geesthacht

(3) Cornec, A., Erweiteres Engineering Treatment Model (ETM/2-93) zur analytischen Beschreibung von Bauteilfließkurven dargestellt an einer Mittenriß-scheibe für die Ver-schiebung CMOD für idealisierte Werkstofffließkurven aus zwei Potenzgesetzen (DPWPL). Technical Note GKSS/WAW/93/11, 1993, GKSS Research Center Geesthacht

(4) Cornec, A., Verifizierungsbeispiel zum erweiterten Engineering Treatment Model (ETM/2-93) am Beispiel einer Mittenrißscheibe aus dem Werkstoff StE 460. Technical Note GKSS/WAW/93/12, 1993, GKSS Research Center Geesthacht

(5) GKSS Displacement Gauge Systems for Applications in Fracture Mechanics. GKSS Research Centre, 1992

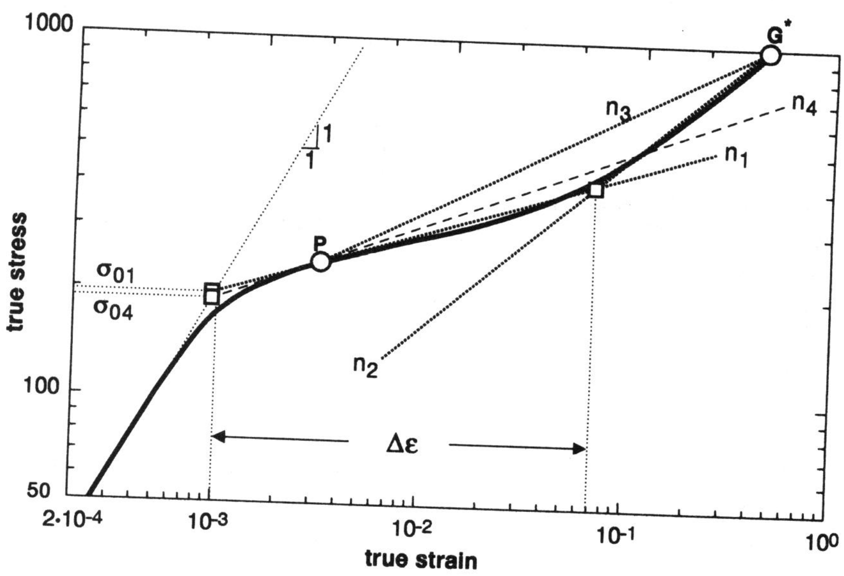

Fig. 1: Tensile stress-strain material curve

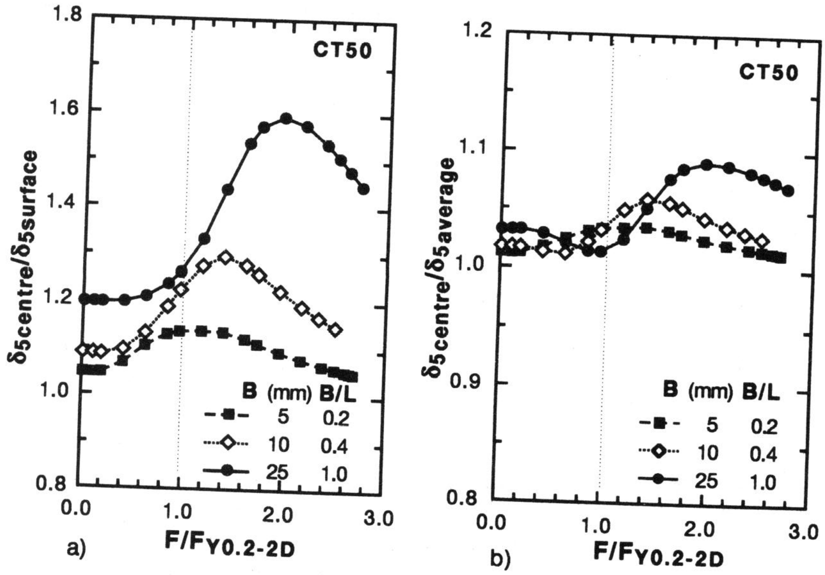

Fig. 2: Behaviour of δ_5 in a 3D CT specimen during loading

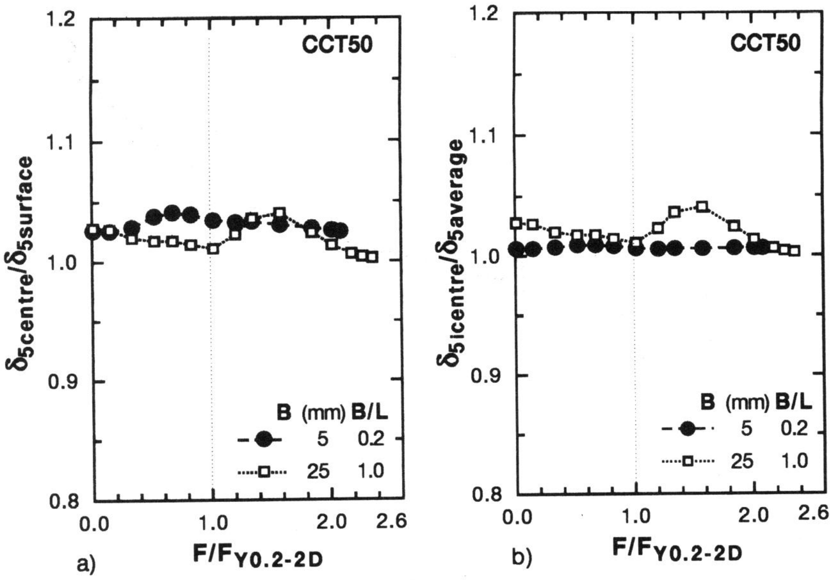

Fig. 3: Behaviour of δ_5 in a 3D CCT specimen during loading

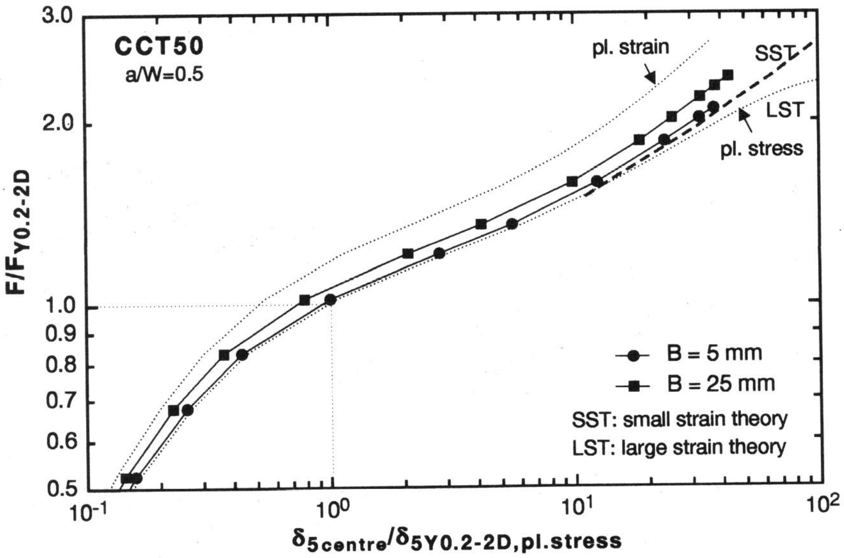

Fig.4: Comparison of 3D and 2D δ_5 driving force behaviour for CCT specimens

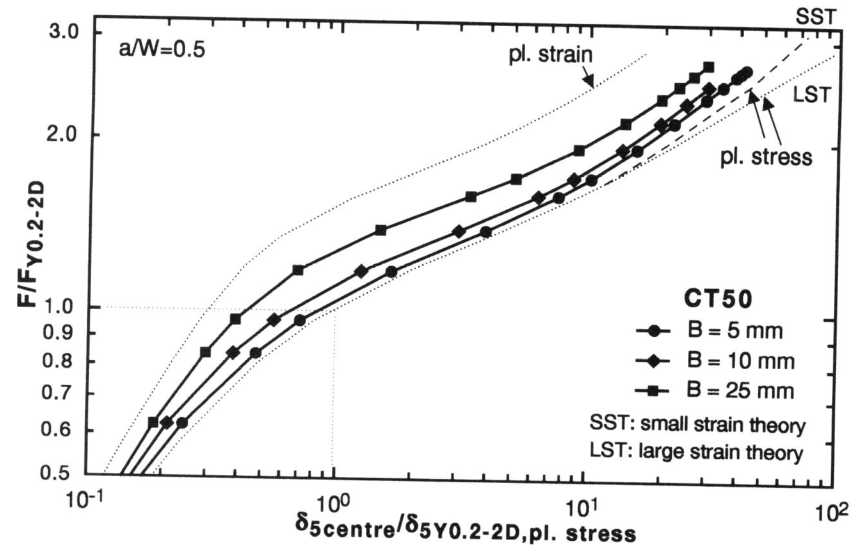

Fig. 5: Comparison of 3D and 2D δ_5 driving force behaviour for CT specimens

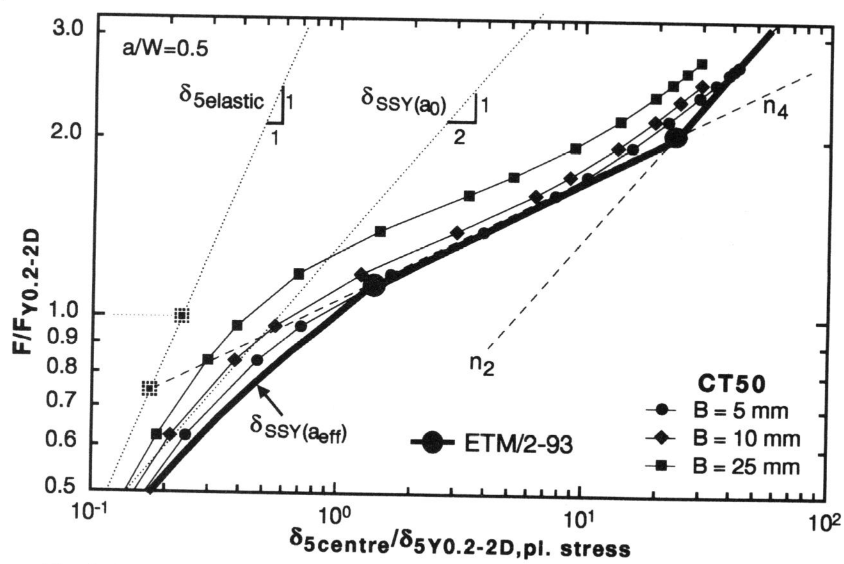

Fig. 6: Application of the ETM/2-93 version to the 3D CT specimens describing analytically the δ_5 driving force